**Cephalic biomechanics underpins the evolutionary success of trilobites**

*by* JORGE ESTEVE[1*], JORDI, MARCÉ-NOGUÉ[2, 3, 4], FRANCESC PÉREZ-PERIS[5] *and* EMILY RAYFIELD[6]

[1] Jorge Esteve [jv.esteve@uniandes.edu.co]. Departamento de Geociencias, Facultad de Ciencias, Universidad de los Andes, Bogotá, Colombia

[2] Jordi, Marcé-Nogué [jordi.marce@urv.cat]. Department of Mechanical Engineering, Universitat Rovira i Virgili, Tarragona, Spain

[3] Centre for Natural History, University of Hamburg, Hamburg, Germany

[4] Institut Català de Paleontologia M. Crusafont, Universitat Autònoma de Barcelona, Cerdanyola del Vallès, Barcelona, Spain

[5] Francesc Pérez-Peris [Francesc.PerezPeris@unil.ch]. Institute of Earth Science, University of Laussane, Géopolis, CH-1015 Laussane, Switzerland.

[6] Emily Rayfield. [e.rayfield@bristol.ac.uk]. School of Earth Sciences, University of Bristol, UK.

*Corresponding author

**Abstract**

Arthropods (i.e. insects, spiders, crustaceans, myriapods and others), are the most successful Phanerozoic animals. The group are characterised by the possession of a segmented body, jointed limbs and a hard cuticle that is episodically moulted. One highly successful, but now extinct, group of arthropods are the trilobites. Trilobites underwent episodic moulting (ecdysis), and most trilobites possess facial sutures, lines of weakness in the cephalon, via which the exuviae is shed and the animal emerges. However, zones of weakness appear to represent a structural trade-off or constraint, particularly during burrowing behaviours; sacrificing a consolidated head region useful in burrowing for the ability to moult. Here we reconcile this trade-off by using biomechanical modelling to demonstrate that facial sutures exist in regions of low stress during the application of burrowing loads. Furthermore, facial sutures and the structure of the cephalon enable sutured trilobites to withstand greater stresses than their non-suture counterparts. We suggest that this ability to withstand greater burrowing loads enabled trilobites to successfully invade bioturbated and more consolidated sediments of the Cambrian Sediment Revolution, thus facilitating their diversification in the Cambrian and Ordovician and contributing to the evolutionary success of this iconic arthropod group.

TRILOBITES represent the best known of any marine Palaeozoic arthropod group thanks to their rich fossil record and exoskeleton development (Hughes 2007*a*), along with information on their geographical and geological occurrence (Álvaro *et al.* 2013) non-biomineralized tissues (Hopkins *et al.* 2017), and associated trace fossils (Seilacher 1985). The group is characterised by the presence of three longitudinal lobes that run from the anterior to the posterior length of the body and three distinct body regions: a head region (cephalon), thorax with serially-repeating segmented limbs and gills, and a tail (pygidium). The presence of advanced compound eyes and the capacity to enrol protecting their bodies are thought to have contributed to the group's success (Hughes 2007*a*; Esteve *et al.* 2011; Strausfeld *et al.* 2016). Attempts to understand the pattern and timing of trilobite evolution have identified two important radiations — during the Cambrian Explosion (Gaines 2014), and the Ordovician Great Biodiversification event — (Adrain *et al.* 1998). Here, we focus on the first trilobite radiation, particularly the early Cambrian where trilobites with and without facial sutures coexisted (Hughes 2007*a*). The facial suture is a unique structure that assisted trilobites during moulting, acting as a zone of weakness along which the cephalon breaks apart during the moult cycle (Fig. 1A-D). Early Cambrian trilobites (i.e. suborder Olenellina) lack facial (dorsal) sutures whilst the presence of facial sutures is considered a characteristic of suborder Redlichiina and all higher trilobites (Jell 2003; Hughes 2007*b*). Although the facial sutures were only functional during moulting, their traces are seen in entire trilobites and constitute preferential lines of weakness (Daley & Drage 2016; Corrales-García *et al.* 2020). It is unclear what factors drive the trade-off between the advantages of having a facilitator for moulting, and the disadvantage of a potentially weak zone. We tackled this problem by focusing on a particular feature of early trilobite behaviour that clearly has adaptive significance observed in both trilobite radiations – feeding habit. The absence of mouth parts and chelate legs and the similarity between the outer ramus of some trilobites and the limbs of some crustaceans suggest that some trilobites were microphagous (Seilacher 1985). However, clear evidence of macrophagous feeding habits already existed in the lower Cambrian (Jensen 1990). *Cruziana* and *Rusophycus* have been interpreted as trilobite burrows or furrows made for trilobites for feeding, including Olenellina and Redlichiina, and other post Cambrian trilobites (Seilacher & Crimes 1969; Crimes 1975*a*; Seilacher 1985; Tarhan *et al.* 2012; Selly *et al.* 2016). Therefore, early feeding habits in trilobites (microphagous and macrophagous feeding, see Fortey & Owens 1999) involved a burrowing or furrowing activity. Here we use the general term "burrow" for the interaction between the trilobites and the substrate, in the context of this research burrow does not mean necessarily a deep excavation; see Crimes (1975*b*, *a*) for a nomenclature discussion about burrows and furrows in trilobites and more recent work about the formation of this traces by Kesidis *et al.* (2019). Burrowing places a stress on the cephalon. Consequently, a putative weak surface, like the facial suture, appears unfavourable for such a mode of life, yet facial sutures persist in most trilobite lineages. Here we use finite element analysis (FEA) to calculate stress in

the trilobite cephalon to assess the mechanical behaviour of the lateral and anterior border (doublure) and the genal field of the trilobite cephalic shield during burrowing, to determine whether the suture presents a mechanical trade-off or constraint between facilitating moulting and structural strength required for burrowing.

## MATERIAL AND METHOD

*Reconstruction of the models*

Figure 1A-H shows a reconstruction of the trilobites *Agraulos* and *Holmia* indicating the main morphological features of the cephalon and the terminology used in this work. The cephalic head of 27 different trilobite species with and without facial sutures were analysed as planar 2D models in FEA using the software ANSYS v.17.1 for Windows 7 (64-bit system).

The cephalic heads were oriented for photography in horizontal position and with the posterior border parallel to the posterior margin of the photography field. Digital images for all specimens were captured under bright-field illustration using a Leica DFC 500 digital camera mounted to a Stereoscope Leica M205-C. All images were processed in Adobe Photoshop CS 4.

After this, the steps to generate the digital models from the images, based on Fortuny *et al.* (2012), are as follows:

1.  The reconstructions were made on the basis of the best specimens (i.e. complete cephala) (electronic supplementary material, Esteve et al. 2020, Table S1), using Adobe Illustrator CS5. Reconstructions of the lateral and anterior border (i.e. doublure, Fig. 1) were made using known ventral sides. When the ventral sides were unknown or poorly known we used the paradoublural line, which is a furrow, flexure, or ridge on dorsal exoskeleton of cephalon, conformable with the inner edge of doublure.

2.  Thin sections and/or polished slabs were used to measure the thickness of the cuticle. When thin sections or polished slabs were not available for some reason (e.g. museum material or scarce specimens), broken sclerites were used. Cuticles present a heterogeneous thickness; thereby average measures were used in the models.

3.  Smoothed planar surfaces of the cephala were generated in Rhinoceros v.5.0 (McNeel & Associates), the burrowing force was placed in the axial one third of the maximum cephalic width and the fixed displacement was placed by the articulation between the cephalon and the first trunk segment.

4.  The FEA model generation, as well as the stress distribution results for each cephala, were performed in ANSYS v.17.1

*Finite Element Analysis (FEA)*

In the present study, a plane stress analysis was carried out, in which the analysed structural elements have one dimension (i.e. thickness) smaller than the other two, thus the stresses are negligible with respect to the smaller dimension. FEA enables the observation of stress and strain distribution patterns and magnitudes by simulating loadings and forces involved in a biomechanical situation. Here we used plane models of the cephalic shields belonging to different Cambrian trilobite genera and calculated von Mises stress patterns using plane elasticity (Mase & Mase 1999). Plane models are characterized by an area with a constant thickness and have been certified that in a FEA comparative analysis provide good results (Morales-García *et al.* 2019).

The FEA models of the cephalic head were meshed using 8-node quadrilateral plane elements (QUAD8), creating a quasi-ideal mesh (QIM) (Marcé-Nogué *et al.* 2016). This particular mesh combines sufficient mesh density to capture the variations in the stress patterns, thus guaranteeing stable results when considering that a high-quality mesh should have a high level of homogeneity in the size of its elements in order to assure that the subsequent statistical analyses are not affected by the size of each element. The number of nodes and elements of each trilobite head model can be found in Esteve et al. (2020), Tables S2 and S3.

The thickness of the model was assumed to be constant throughout the genal field and constant with a different value in the lateral and anterior border due to the doublure (electronic supplementary material Table S2 shows the average thickness used in each model). All the models have been created with a width of 25 mm measured between posterolateral edges of the free checks, which is a reasonable measurement for the cephalic shield of all studied genera since all of them reach such a size in their mature stage (i.e. holaspid), including the smallest genera (e.g. *Agraulos, Schophaspis*). Isotropic, homogeneous and linear elastic properties were assumed based on average calcite properties: E [Young´s modulus] = 75 GPa and v [Poisson ratio] = 0.31.

*Burrowing simulation and scaling the force*

Boundary conditions were defined and placed to represent the loads and fixed displacements that the cephalon experiences during burrowing feeding. A fixed boundary condition ('fixed displacement', Fig. 1I) fixes the cephalic shield at the trunk.

Related with the applied loads, when comparing the biomechanical performance of different FEA models of different taxa, the differences in size can be considered and can be removed applying an appropriate value of force in each model. This is a well-known procedure that was described ten years ago based on the homothetic transformations by Dumont et al. (2009). However, the work of Dumont *et al.* (2009) is focused in three-dimensional models and there is a lack of how we should proceed when we are working with plane FEA models. This is important, because plane models are not two-dimensional models. In continuum mechanics, plane

elasticity refers to the study of particular solutions of the general elastic problem in bodies that are geometrically mechanical prisms (an area with a constant thickness) and depending on how these prisms are we can establish plane stress, plain strain and axisymmetric problems. So, they are surfaces with thickness that are decoupled in the equations and this particularity must be considered when applying the equations proposed by Dumont. For this reason Marcé-Nogué *et al.* (2013) developed appropriate equations that should be used for this kind of problem, calling the procedure a "quasi-homothetic transformation" because it decouples thickness and surfaces instead of combining all together in the equations.

The focus of the present study was the comparison between these models, hence an arbitrary burrowing force of 1 N was applied in the reference model *Burlingia*. For the rest of the models under study, a proportional force based on their size differences was calculated using a quasi-homothetic transformation (Marcé-Nogué *et al.* 2013). But, considering that the head shield presents two separate structures (i.e. the doublure throughout the anterior and lateral borders and the genal field, see Fig. 1), the thickness of each cephalon was assumed to be constant in two different parts of the cephalon: the genal field and the lateral and anterior border, i.e. the doublure (Fig. 1). The quasi-homothetic method cannot be used in planar models with two different regions with different thickness each, as our case. Therefore, we performed two different analyses scaling the force respectively in each case and analysing each region separately (See the value of the forces in Esteve et al. 2020, Table S2):

Analysis I) In order to compare the genal field (fixed and free checks) of the head shield, the burrowing force was calculated scaling from the area and average thickness of the genal field.

Analysis II) In order to compare the anterior and lateral borders of the cephalic heads, the burrowing force was calculated scaling from the area and thickness of the anterior and lateral borders.

Scaling the forces allows an appropriate comparison between stress results, although it is important to notice that this is not correcting for any differences in shape effects that might be involved. Size and function are intertangled because many biological variables correlate with size, thus correcting for those differences in shape would remove some of the differences in shape related to function, which are aspects we are interested in. Therefore, when interpreting the FEA results, it is relevant to bear in mind that, in spite of the scaling, shape differences have to be considered.

*Analysis of von Mises Stress*

The observed differences in von Mises stress distribution patterns provide clues on different aspects of burrowing of the analysed species (Figs 2, 3, Esteve et al. 2020, figs S1) in relation to

the type of sutures that they bear. However, a quantitative single measurement of the relative strength of the structure under study was preferred to summarise and compare the strength of each whole model. The most common approach is to compute average von Mises stresses or other quantitative metrics such as median stress or the percentile values of stress, e.g. 75th percentile (M75), 95th percentile (M95) of each FEA model considered. Even though this approach has been used previously in palaeobiological studies (Gil et al. 2015; Tseng & Flynn, 2015; Figuerido et al. 2014; Neenan et al. 2014; Lautenschlager 2017; Blanke et al. 2017; ), we apply here the proposed quasi-ideal mesh (QIM) method, which allows us to study the percentile values of stress (M25, M50, M75 and M95) as a basis for quantitative analysis(Zhou *et al.* 2019; Marcé-Nogué *et al.* 2020). In order to ensure a QIM, we computed the required errors Percentage Error of the Arithmetic Mean (PEofAM) and the Percentage Error of the Median (PEofM) to be sure that they fulfil the requirements (PEofAM < 2% and PEofM < 5%). For a better description, see details of the method in Marcé-Nogué *et al.* (2016) . The distribution of stress in each trilobite cephalon model using boxplots for both analyses I and II in the genal field and the lateral and anterior border.

It must be noted that a singular and unusually high stress can appear where the boundary conditions are set. This numerical singularity is a consequence of the applied mathematical approach, inflated by the constraints imposed on the model (Marcé-Nogué *et al.* 2015) and consequently it is not related to any biological process. In these areas, stresses have the tendency to increase in value towards infinity; therefore, results of these areas should not be considered in the quantitative analysis of stress. Following the suggestions of Walmsley *et al.* (2013), the analysis of the 95th percentile of the boxplot (M95) as a peak value avoids these artificial high values.

*Statistical analysis*

By applying a Shapiro-Wilk test we checked the normality assumption for the stress values for each group. Groups are divided into two categories i) trilobites with facial sutures and without facial sutures and ii) four taxonomical groups: Olenelliina, Redlichiina, Ptychopariina and Asaphina. The results showed that none of these groups followed a normal distribution and that non-parametrical analysis should be used.

Dunn's test of multiple comparisons with Bonferroni correction was used to test differences between the morphological results and the FEA results between groups (Dunn 1964). As indicated above, we used the percentile values of stress of each species: 25th, 50th, 75th and 95th. The Interquartile Range (IQ) was also computed for each species, giving a measure of statistical dispersion, being equal to the difference between 75th and 25th percentiles, and therefore

displaying how the stresses are spread inside the cephalic head of the trilobites, low IQR means that the values of stress inside the head are more homogeneous than for high IQ, which means that low and high values of stress are coexisting in the cephalic head. To study the relationship between stress in the inner part of the head (i.e. genal area) and the outer part (i.e. the doublure), we divided the value of stress in the outer part by the same value in the inner part. All the statistical analysis were carried out with R 3.3.3 (http://www.R-project.org/).

**RESULTS**

Twenty-seven finite element models were created, 12 taxa without facial sutures (i.e. Olenellina) and 15 taxa with facial sutures (i.e. Redlichiina, Pthycopariida and Asaphida). During simulated burrowing, FEA results showed a correlation between areas of lower stresses at the location of the free cheek in trilobites with facial suture, and lower stress and the extraocular area in those without a facial suture (Figs 2-3). These results point to a structural feature in the cephalic shield of trilobites with and without facial sutures to withstand forces produced during burrowing by minimising stress in the position where the dorsal facial sutures are situated. It is noteworthy that the dorsal facial suture in redlichiid, ptychopariid and asaphid trilobites separates the free cheek of the genal field in the limit between higher and lower stresses (Fig. 2, Esteve et al. 2020, fig. S1).

The Figure 4 summarises the strength of the whole model and shows the difference between trilobites with facial sutures and those without facial sutures. We calculate the median stress and the 95th percentile stress as a peak value, for each trilobite model. Comparing these values between species shows that species with facial sutures have significant differences (Fig. 4) in the stiffness of the head structure compared to those species without facial sutures. The stress values in trilobites with facial sutures decreases in the genal field and increase in the lateral and anterior border. This means that burrowing trilobites without facial sutures may reach calcite failure stress in the genal field before those with facial sutures (Côté *et al.* 2015). By inference, trilobites with facial sutures could therefore burrow through more consolidated (i.e. harder) substrates. The Interquartile Range (IQR, difference between 75th and 25th percentile value of stress in each species) was also calculated (Fig. 4). The IQR displays how the stress is spread inside the lateral and anterior border and the genal field of the trilobites. Thus, those models showing greater homogeneity with respect to stress are better adapted to resist burrowing loadings, consequently heterogenous distribution of stress in the cephalic head suggests a poorer adaptation for burrowing. In trilobites with a facial suture, the genal field shows a wider IQR range than the doublure, suggesting more homogeneous stress in the later. The anterior and lateral border in trilobites with facial sutures are interpreted as more efficient against external load than

non-suture taxa because weak points (localised stress peaks) are not present in the structure. Nonetheless, trilobites without facial suture present a wider IQR range suggesting a very heterogeneous distribution of stress, with lower and higher stress values coexisting inside the structure. In addition, we assess the relationship between the genal field and the lateral and anterior border of the cephalic shield. The median and the 95th percentile ratios quantify the differences in stress between the genal field and the doublure of the cephalic shield. Ratios close to 1 mean that the whole structure (i.e. cephalic shield) is very homogenous with similar stress distributions, therefore more efficient against external stress. Trilobites without facial sutures have smaller ratios, hence greater differences in stress between the genal field and the doublure. We interpret this heterogeneous design as trilobites without facial sutures were less efficient at burrowing.

As the likelihood of cephalon fracture is equivalent for all taxa, since the material composition is (apparently) the same (Wilmot 1990; Fortey & Wilmot 1991), trilobites with lower stress values in the cephalon are able to withstand greater burrowing forces before failure. Furthermore, trilobites with dorsal facial sutures show narrower IQR ranges than trilobites without dorsal facial sutures, and in these latter forms the genal field is also more fragile. This implies there are areas in the head where more biomineralized exoskeleton is present than needed to withstand burrowing loads. Contrariwise, the short IQR range in sutured trilobites reflects an efficient distribution of biomineralized exoskeleton to withstand burrowing load. Finally, the median and the 95th percent ratios point out a more efficient design in trilobites with facial sutures.

In order to explore trends in cephala mechanics and burrowing capability and how this relates to increased bioturbation, we divided our sampled taxa into four groups, the suborders Olenelliina, Redlichiina and Ptychopariina exclusively from the Cambrian, and the suborder Asaphina, a Cambrian-Ordovician clade, but represented here by only stratigraphically early genera from the Cambrian. Burrowing-induced stress shows no significant difference among Olenelliina, Redlichiina and Ptychopariina (Fig. 5). However, Asaphina trilobites have significantly higher stress in the lateral and anterior border and lower stress in the genal field compared to Olenelliina, Redlichiina and Ptychopariina trilobites. The IQR ranges in both lateral and anterior border and genal field are also significantly narrower in asaphid trilobites compared with the other groups. In addition, the median and the 95th percent stress ratios are closer to one, suggesting that asaphids had the most homogenous accommodation of cephalon stress of all four trilobite groups. All these parameters suggest a more appropriate design for burrowing in Asaphina trilobites than the typical Cambrian trilobites. The functional modification to the head of Asaphina trilobites may explain the success of this group in the Ordovician. An increase in depth and intensity of bioturbation through the Ordovician has been ascribed to the soft-bodied metazoan radiation (Mángano & Buatois 2017; Van De Velde *et al.* 2018), but trilobites provide

evidence that this was also at least partially the result of trilobite burrowing during the Cambrian and especially in Ordovician carbonate settings (e.g. asaphid trilobites as trace-makers of *Thalassinoides*, see Cherns *et al.* 2006).

**DISCUSSION**

Lower patterns of stress in the genal field are present at the location of the facial sutures in those trilobites with dorsal facial sutures and same lower stress pattern in the genal field is observed in trilobites without dorsal facial sutures. This fact presages a trade-off between lower stress pattern and allocation of the facial sutures this low stress position in the genal field. Facial sutures in the genal field assisted trilobites to moult their exoskeleton in a high number of configurations (e.g. Corrales-García *et al.* 2020). Likewise, ollenellids had a circumocular suture in the genal field which appears in some ollenellids during late meraspid or early holaspid stages (Palmer 1957; Webster 2015). Webster (2015) described the visual surface as missing in some early meraspid cephala suggesting that the circumocular suture was functional at this stage; however Palmer & Gayle (1971) illustrated an holaspid mould of *Bristolia* in which the eye surface is outlined and preserved therefore not functional at that stage. Therefore, function of the circumocular suture may or may not be used for moulting since also it is a common feature in some other redlichiids with a dorsal facial suture (Dean & Rushton 1997). Anyway, in order to moult trilobites with and without dorsal facial sutures (i.e. Cambrian trilobites and likely other post-Cambrian trilobites) flexed the body prying the anterior cephalic border against the seafloor to open facial sutures (McNamara & Rudkin 1984; McNamara 1986; Whittington 1990). This technique for moulting could cause injures (Owen 1985) and especially in the anterior cephalic edge (anterior border) where trilobites without facial sutures (i.e. ollenelids) open the cephalon during ecdysis (Hupé 1952, pp. 120-122; Whittington 1989, pp. 137-138; Webster 2015). Injures in the anterior border have been documented recently in trilobites by Bicknell & Holland (2020) and Bicknell & Pates (2020) with similar biomechanics properties of modern arthropods (Bicknell *et al.* 2018). These authors also show comparable injures in the ventral side of the anterior border in *Limulus*, which also has a similar burrowing behaviour (see Eldredge 1970; Fisher 1975). Thus, allocating the facial sutures to the dorsal surface reduces the probability of damage the sutures if they are allocated in the anterior border during moulting but also during normal non-moulting behaviour. On the other hand, despite the consistent body plan in trilobites, moulting behaviours described in trilobites have been highly variable throughout their evolutionary history and especially diverse during the Cambrian (Daley & Drage 2016; Drage 2019; Corrales-García *et al.* 2020). This high disparity in moulting behaviour can be partially explained thanks to the shift of the position of ecdysis sutures from the edge in ollenelids to the dorsal surface in other trilobites. Once the facial suture is allocated in the dorsal surfaces (just where the low stresses take place in the genal field)

different morphologies can be achieved (i.e. opisthoparian proparian, gonatoparian) and subsequently highly flexible moulting behaviour can be developed in the Cambrian to establish trilobites in new and diverse ecological niches (Drage 2019).

The quantitative indicators of von Mises stress distributions in trilobites with and without facial sutures present an antagonistic behaviour in the trilobite heads. The stiffness of the lateral and anterior border in trilobites with facial sutures is higher because the contact with the sediment during the burrowing or during the moulting is performed by this part of the carapace. Meanwhile, the stress values in the genal field are lower, since there is not direct contact with the sediment during the first moment of both behaviours (burrowing and moulting). However, trilobites without facial sutures display higher stress values in the genal field of the head and lower values in the lateral and anterior border given the need to push the sediment with the anterior border during the moulting.

We interpret this antagonistic behaviour as an ecological innovation related to the Cambrian Substrate Revolution (Bottjer 2010). Neoproterozoic-type substrates stabilized by microbial mats were replaced throughout the Cambrian Series 2 and Miaolingian Series by unconsolidated soft substrates with a well-developed bioturbated layer (McIlroy & Logan 1999; Bottjer 2010; Gougeon et al. 2018). These microbial mats were likely difficult or impossible for early benthic animals to penetrate (McIlroy & Logan 1999; Bottjer 2010). In addition, the combination of the microbial mats and a lack of infaunal bioturbation would have prevented aeration of the sediment, allowing an oxic-anoxic boundary to develop in the sediment close to the seafloor surface (McIlroy & Logan 1999). As a result, all metazoan activities, including trilobites, likely occurred on the top surface of mats, within mats, or immediately beneath them but not at greater depths. Deep burrowing was unnecessary, which links to more fragile genal fields and the biomechanical properties of the cephalon. The biomechanical design of the early trilobites without facial sutures like ollenelids (with lower stress values in the lateral and anterior border), may have allowed them to penetrate slightly under the sediment or beneath the microbial mats either to feed on them or hunt prey. During the Cambrian Series 2 and Miaolingian Series, the unconsolidated soft substrates stabilized by microbial mats disappeared and the first deep bioturbators appeared, acting as ecosystem engineers (Mcilroy et al. 2005; Gougeon et al. 2018). Manton (1954, p. 345) and Manton (1958, p. 493) showed how the length of trunk rings (and consequently the body size) and the stride are important features for burrowing since a slow gait with short strides (likely as in Cruziana) help to burrow in diplopods. Therefore, the diversity in the axial rings morphology, the number of trunk segments and likely the possibility to modify the gait linked with a more efficient head biomechanics in trilobites with dorsal facial suture allowed improve burrowing. Sediment mixing became intense in the late Cambrian Series 2 facilitating the expansion of aerobic bacteria, increasing the rate of organic matter decomposition and the

regeneration of nutrients at depth within the substrate (McIlroy & Logan 1999; Boyle *et al.* 2014; Mángano & Buatois 2014, 2017; Gougeon *et al.* 2018). The inferior load-resistance in the head of ollenelids may have prevented burrowing of the well-bioturbated, deeper and harder substrates. This shift towards well-bioturbated and harder substrates associated with an increase in predation may therefore be the underlying causes of the decline and extinction of ollenelids in the Cambrian Series 2. Besides, dorsal facial sutures and subsequently modifications were highly success in this group for moulting and the lack of appropriate moulting mechanics could also play an important role in the extinction of this group.

Here, we demonstrate that the evolution of cephalic shield shapes and facial sutures may have facilitated ease of trilobite moulting and the ability to adapt to and invade a new, infaunal, ecological niche. Modified cephalon design and resistance to burrowing loads therefore enabled trilobites to capitalise on bioturbated and oxygenated infaunal habitats during the Cambrian Substrate Revolution. This successful shallow bioturbation behaviour of trilobites, joined with other bioturbated animals, was a major driver of the following "explosion" - the Great Ordovician Biodiversification event - and affected the biogeochemical cycling during the whole Palaeozoic (McIlroy & Logan 1999; Mángano & Buatois 2014, 2017; Gougeon *et al.* 2018).

**CONCLUSIONS**

We can highlight the following conclusions of our study:

1. Dorsal facial sutures allocated in low stress positions in the genal field improved the process of ecdysis in trilobites, driving the high diversity of these arthropods recorded during the Palaeozoic.
2. Biomechanics of the head in of non-facial sutured trilobites shows adaptation to superficial burrowing in substrates stabilized by microbial mats.
3. Head design of facial sutured trilobites allowed them to bioturbate Cambrian substrates and later trilobites evolved new infaunal ecological niches during the GOBE.

**Author´s contribution.** J.E. and J.M-N performed the research; J.E. made the reconstructions;

F.P.P made the smoothed planar surfaces; J.M-N carried out the FEA; J.M-N and E.R. discussed the FEA analysis; J.E. and E.R. discussed the paleobiologic significance of the results; J.E., J.M-N and E.R. wrote the paper; all the authors reviewed the manuscript.

## DATA ARCHIVING STATEMENT

Data for this study are available in the Dryad Digital Repository:

https://datadryad.org/stash/share/U-7CENTMg-QZU2f0qGAxXHI3zj1e4McTG-qVj44qttQ.

## References

ADRAIN, J. M., FORTEY, R. A. and WESTROP, S. R. 1998. Post-cambrian trilobite diversity and evolutionary Faunas. *Science*, **280**, 1922–1925.

ÁLVARO, J. J., AHLBERG, P., BABCOCKL.E., L. E., BORDONARO, O. L., CHOI, D. K., COOPER, R. A., ERGALIEV, G. K. H., GAPP, I. W., POUR, M. G., HUGHES, N. C., JAGO, J. B., KOROVNIKOV, I., LAURIE, J. R., LIEBERMAN, B. S., PATERSON, J. R., PEGEL, T. V., POPOV, L. E., RUSHTON, A. W. A., SUKHOV, S. S., TORTELLO, M. F., ZHOU, Z. and ZYLIŃSKA, A. 2013. Global Cambrian trilobite palaeobiogeography assessed using parsimony analysis of endemicity. *Geological Society Memoir*, **38**, 273–296.

BICKNELL, R. D. C. and PATES, S. 2020. Exploring abnormal Cambrian-aged trilobites in the Smithsonian collection. *PeerJ*, **8**, e8453.

——— and HOLLAND, B. 2020. Injured trilobites within a collection of dinosaurs: Using the royal tyrrell museum of palaeontology to document cambrian predation. *Palaeontologia Electronica*, **23**, 1–11.

———, LEDOGAR, J. A., WROE, S., GUTZLER, B. C., WATSON, W. H. and PATERSON, J. R. 2018. Computational biomechanical analyses demonstrate similar shell-crushing abilities in modern and ancient arthropods. *Proceedings of the Royal Society B: Biological Sciences*, 20181935.

BOTTJER, D. J. 2010. The cambrian substrate revolution and early evolution of the phyla. *Journal of Earth Science*, **21**, 21–24.

BOYLE, R. A., DAHL, T. W., DALE, A. W., SHIELDS-ZHOU, G. A., ZHU, M., BRASIER, M. D., CANFIELD, D. E. and LENTON, T. M. 2014. Stabilization of the coupled oxygen and phosphorus cycles by the evolution of bioturbation. *Nature Geoscience*, **7**, 671–676.

CHERNS, L., WHEELEY, J. R. and KARIS, L. 2006. Tunneling trilobites: Habitual infaunalism in an Ordovician carbonate seafloor. *Geology*, **34**, 657–660.

CORRALES-GARCÍA, A., ESTEVE, J., ZHAO, Y. and YANG, X. 2020. Synchronized moulting behaviour in trilobites from the Cambrian Series 2 of South China. *Scientific Reports*, **10**, 14099.

CÔTÉ, A. S., DARKINS, R. and DUFFY, D. M. 2015. Deformation twinning and the role of amino acids and magnesium in calcite hardness from molecular simulation. *Physical Chemistry Chemical Physics*, **17**, 20178–20184.

CRIMES, T. P. 1975*a*. Trilobite traces from the Lower Tremadoc of Tortworth. *Geological Magazine*, **112**, 33–46.

CRIMES, T. P. 1975*b*. The production and preservation of trilobite resting and furrowing traces. *Lethaia*, 35–48.

DALEY, A. C. and DRAGE, H. B. 2016. The fossil record of ecdysis, and trends in the moulting behaviour of trilobites. *Arthropod Structure and Development*, **45**, 71–96.

DEAN, W. T. and RUSHTON, A. W. A. 1997. Subfamily Paradoxidoidea. *In* R.L. KAESLER (ED.) (ed.) *Treatise on Invertebrate Paleontology, Part O, Revised. Arthropoda 1, Trilobita 1 (Revised)*, Geological Society of America-University of Kansas, Boulder-Lawrence., 470–481. pp.

DRAGE, H. B. 2019. Quantifying intra-and interspecific variability in trilobite moulting behaviour across the Palaeozoic. *Palaeontologia Electronica*, **22**, 1–39.

DUMONT, E. R., GROSSE, I. R. and SLATER, G. J. 2009. Requirements for comparing the performance of finite element models of biological structures. *Journal of Theoretical Biology*, **256**, 96–103.

DUNN, O. J. 1964. Multiple Comparisons Using Rank Sums. *Technometrics*.

ELDREDGE, N. 1970. Observations on burrowing behavior in Limulus polyphemus (Chelicerata, Merostomata), with implications on the functional anatomy of trilobites. *American Museum Novitates*, 1–17.

ESTEVE, J., HUGHES, N. C. and ZAMORA, S. 2011. Purujosa trilobite assemblage and the evolution of trilobite enrollment. *Geology*, **39**, 575–578.

———, MARCÉ-NOGUÉ, J., PÉREZ-PERIS, F., and RAYFIELD. E. 2021. Data from: Cephalic biomechanics underpins the evolutionary success of trilobites. *Dryad Digital Repository*. https://doi.org/10.5061/dryad.r2280gb9s
.

FISHER, D. C. 1975. Swimming and burrowing in Limulus and Mesolimulus. *Fossils and Strata*, **4**, 281–290.

FORTEY, R. A. and WILMOT, N. V. 1991. Trilobite cuticle thickness in relation to palaeoenvironment. *Paläontologische Zeitschrift*, **65**, 141–151.

——— and OWENS, R. M. 1999. Feeding habits in trilobites. *Palaeontology*, **42**, 429–465.

FORTUNY, J., MARCÉ-NOGUÉ, J., GIL, L. and GALOBART, À. 2012. Skull Mechanics and the Evolutionary Patterns of the Otic Notch Closure in Capitosaurs (Amphibia: Temnospondyli). *Anatomical Record*, **295**, 1134–1146.

GAINES, R. R. 2014. Burgess Shale-type Preservation and its Distribution in Space and Time. *The Paleontological Society Papers*, 123–146.

GOUGEON, R. C., MÁNGANO, M. G., BUATOIS, L. A., NARBONNE, G. M. and LAING, B. A. 2018. Early Cambrian origin of the shelf sediment mixed layer. *Nature Communications*, **9**, 1909.

HOPKINS, M. J., CHEN, F., HU, S. and ZHANG, Z. 2017. The oldest known digestive system consisting of both paired digestive glands and a crop from exceptionally preserved trilobites of the Guanshan Biota (Early Cambrian, China). *PLoS ONE*, **12**, e0184982.

HUGHES, N. C. 2007*a*. The Evolution of Trilobite Body Patterning. *Annual Review of Earth and Planetary Sciences*, **35**, 401–434.

———. 2007*b*. Strength in numbers: High phenotypic variance in early Cambrian trilobites and its evolutionary implications. *BioEssays*, **29**, 1081–1084.

HUPÉ, P. 1952. Contribution A L´Étude du Cambrien INférieur et du Précambrien III de LÁnti-Atlas Marocain. 1–292.

JELL, P. A. 2003. Phylogeny of early cambrian trilobites. *Special Papers in Palaeontology*, **70**, 45–57.

JENSEN, S. 1990. Predation by early Cambrian trilobites on infaunal worms - evidence from the Swedish Mickwitzia Sandstone. *Lethaia*, **23**, 29–42.

KESIDIS, G., BUDD, G. E. and JENSEN, S. 2019. An intermittent mode of formation for the trace fossil Cruziana as a serial repetition of Rusophycus: the case of Cruziana tenella (Linnarsson). *Lethaia*, 133–148.

MÁNGANO, M. G. and BUATOIS, L. A. 2014. Decoupling of body-plan diversification and ecological structuring during the Ediacaran-Cambrian transition: Evolutionary and geobiological feedbacks. *Proceedings of the Royal Society B: Biological Sciences*, **281**, 20140038.

——— and ———. 2017. The Cambrian revolutions: Trace-fossil record, timing, links and geobiological impact. *Earth-Science Reviews*, 96–108.

MANTON, S. M. 1954. The evolution of arthropodam locomotoru mechnisms.-Part 4. The structure, habits and evolution of the Diplopoda. *Journal of the Linnean Society of London, Zoology*, **42**, 299–364.

———. 1958. The evolution of arthropodan locomotory mechanisms. Part 6. Hqbits and evolution of the Lysiopetaloidea (Diplopoda), some principles of leg design in Diplopoda and Chilopoda, and limbs structure of Diplopoda. *Journal of the Linnean Society of London, Zoology*, **43**, 487–557.

MARCÉ-NOGUÉ, J., FORTUNY, J., GIL, L. and SÁNCHEZ, M. 2015. Improving mesh generation in finite element analysis for functional morphology approaches. *Spanish Journal of Palaeontology*, 117–132.

———, DE ESTEBAN-TRIVIGNO, S., ESCRIG, C. and GIL, L. 2016. Accounting for differences in element size and homogeneity when comparing finite element models: Armadillos as a case study. *Palaeontologia Electronica*, **19**, 1–22.

———, PÜSCHEL, T. A., DAASCH, A. and KAISER, T. M. 2020. Broad-scale morpho-functional traits of the mandible suggest no hard food adaptation in the hominin lineage. *Scientific Reports*, **10**, 6793.

———, DEMIGUEL, D., FORTUNY, J., DE ESTEBAN-TRIVIGNO, S. and GIL, L. 2013. Quasi-homothetic transformation for comparing the mechanical performance of planar models in biological research. *Palaeontologia Electronica*, **16**, 1–15.

MCILROY, D. and LOGAN, G. A. 1999. The impact of bioturbation on infaunal ecology and evolution during the Proterozoic-Cambrian transition. *Palaios*, **14**, 58–72.

MCILROY, D., CRIMES, T. P. and PAULEY, J. C. 2005. Fossils and matgrounds from the Neoproterozoic Longmyndian Supergroup, Shropshire, UK. *Geological Magazine*, 441–455.

MCNAMARA, K. J. 1986. Techniques of exuviation in Australian species of the cambrian trilobite redlichia. *Alcheringa*, **10**, 403–412.

MCNAMARA, K. J. and RUDKIN, D. M. 1984. Techniques of trilobite exuviation. *Lethaia*, **17**, 153–173.

MORALES-GARCÍA, N. M., BURGESS, T. D., HILL, J. J., GILL, P. G. and RAYFIELD, E. J. 2019. The use of extruded finite-element models as a novel alternative to tomography-based models: A case study using early mammal jaws. *Journal of the Royal Society Interface*, **16**, 20190674.

OWEN, A. W. 1985. Trilobite abnormalities. *Transactions of the Royal Society of Edinburgh, Earth Sciences*, **76**, 255–272.

PALMER, A. R. 1957. Ontogenetic Development of Two Olenellid Trilobites. *Journal of Paleontology*, **31**, 105–128.

PALMER, A. R. and GAYLE, H. D. 1971. A new olenellid trilobite, Biceratops nevadensis, from the Lower Cambrian near Las Vegas, Nevada. *Journal of Paleontology*, **45**, 893–898.

SEILACHER, A. 1985. Trilobite palaeobiology and substrate relationships. *Transactions of the Royal Society of Edinburgh: Earth Sciences*, **76**, 231–237.

——— and CRIMES, T. P. 1969. "European" Species of Trilobite Burrows in Eastern Newfoundland. *In North Atlantic—Geology and Continental Drift*, .

SELLY, T., HUNTLEY, J. W., SHELTON, K. L. and SCHIFFBAUER, J. D. 2016. Ichnofossil record of selective predation by Cambrian trilobites. *Palaeogeography, Palaeoclimatology, Palaeoecology*, **444**, 28–38.

STRAUSFELD, N. J., MA, X., EDGECOMBE, G. D., FORTEY, R. A., LAND, M. F., LIU, Y., CONG, P. and HOU, X. 2016. Arthropod eyes: The early Cambrian fossil record and divergent evolution of visual systems. *Arthropod Structure and Development*, **45**, 152–172.

TARHAN, L. G., JENSEN, S. and DROSER, M. L. 2012. Furrows and firmgrounds: Evidence for predation and implications for Palaeozoic substrate evolution in Rusophycus burrows from the Silurian of New York. *Lethaia*, **45**, 329–341.

VAN DE VELDE, S., MILLS, B. J. W., MEYSMAN, F. J. R., LENTON, T. M. and POULTON, S. W. 2018. Early Palaeozoic ocean anoxia and global warming driven by the evolution of shallow burrowing. *Nature Communications*, **9**, 2554.

WALMSLEY, C. W., SMITS, P. D., QUAYLE, M. R., MCCURRY, M. R., RICHARDS, H. S., OLDFIELD, C. C., WROE, S., CLAUSEN, P. D. and MCHENRY, C. R. 2013. Why the Long Face? The Mechanics of Mandibular Symphysis Proportions in Crocodiles. *PLoS ONE*, **8(1)**, e53873.

WEBSTER, M. 2015. Ontogeny and intraspecific variation of the early Cambrian trilobite Olenellus gilberti, with implications for olenelline phylogeny and macroevolutionary trends in phenotypic canalization. *Journal of Systematic Palaeontology*, **13**, 1–74.

WHITTINGTON, H. B. 1989. Olenelloid trilobites: type species, functional morphology and higher classification. *Philosophical Transactions - Royal Society of London, B*, **324**, 111–147.

———. 1990. Articulation and exuviation in Cambrian trilobites. *Philosophical Transactions of the Royal Society of London. Series B: Biological Sciences*, **329**, 27–46.

WILMOT, N. V. 1990. Biomechanics of trilobite exoskeletons. *Palaeontology*, **33**, 749–768.

ZHOU, Z., WINKLER, D. E., FORTUNY, J., KAISER, T. M. and MARCÉ-NOGUÉ, J. 2019. Why ruminating ungulates chew sloppily: Biomechanics discern a phylogenetic pattern. *PLoS ONE*, **14**, e0214510.

## Figures

**Figure 1**. A-H. Reconstruction of the cephalon of *Agraulos* with facial sutures (A-D) and *Holmia* without facial sutures (E-H). A, E. Reconstruction of the dorsal view. B, F. Reconstruction of the ventral view. C, G. Reconstruction of the dorsal view showing the morphological features used in the text. D, H. Reconstruction of the ventral view showing the morphological features used in the text. I. Free-body diagram of simulated loads during burrowing in the trilobite head.

**Figure 2**. Von Mises Stress distribution in species with dorsal facial sutures, analysed differently under equivalent loads in analysis I (in genal field) and analysis II (in lateral and anterior border).
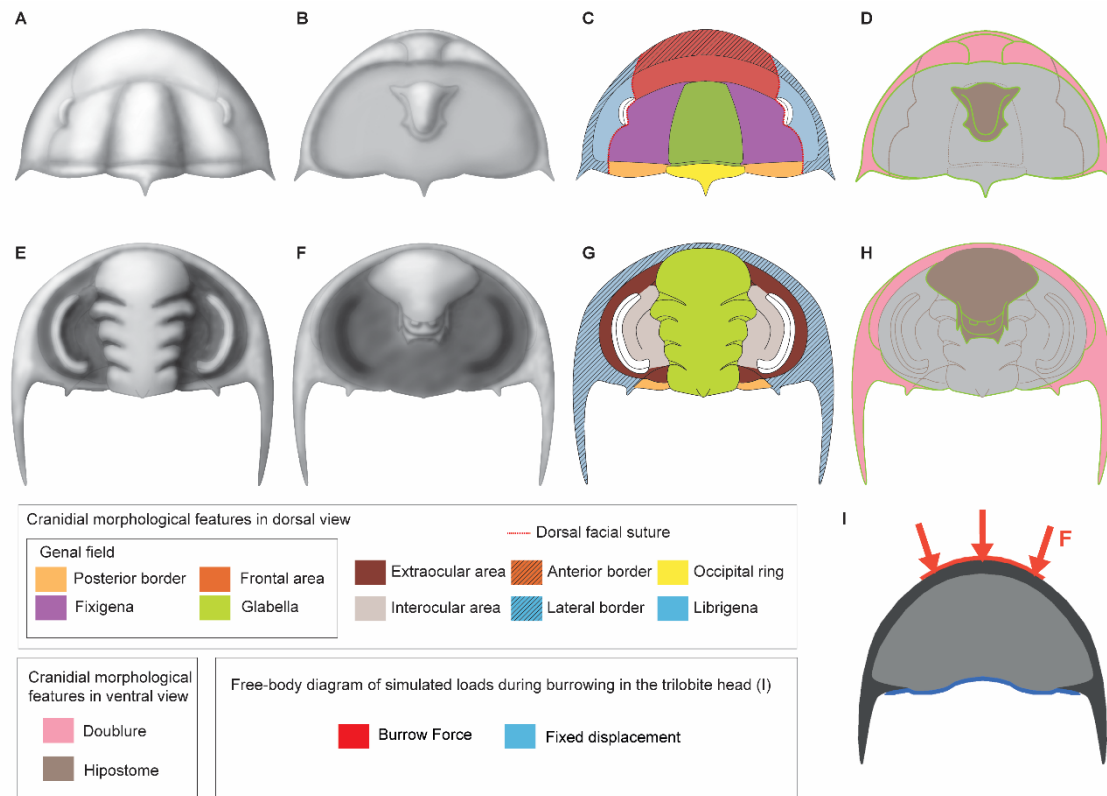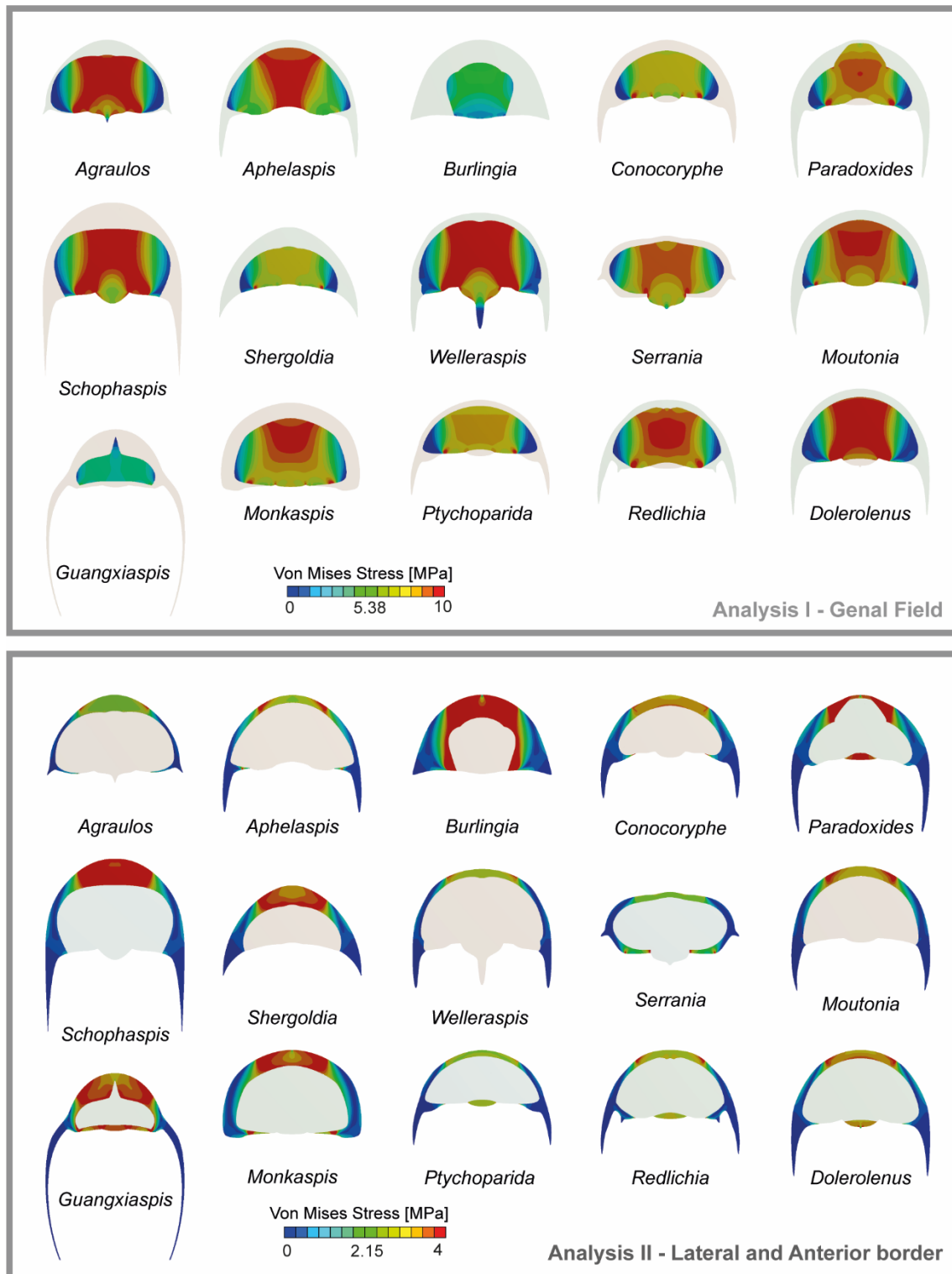
**Figure 3**. Von Mises Stress distribution in species without dorsal facial sutures, analysed differently under equivalent loads in analysis I (in genal field) and analysis II (in lateral and anterior border).

**Figure 4**. Box-plots of the median (M50), peak (M95) stress values and the Interquartile Range (IQR) for each FEA model in the genal field (solved in analysis I) and in the anterior and lateral borders o (solved in analysis II) of all species grouped by the presence or absence of the facial suture. The Ratios are the comparison between the result obtained in the genal field (analysis I) and the anterior and lateral borders (analysis II) of M50 and M95 values. The median is the middle line and the box and whiskers represent the range. F and p-values of the Dunn's test with Bonferroni correction are included in each case.
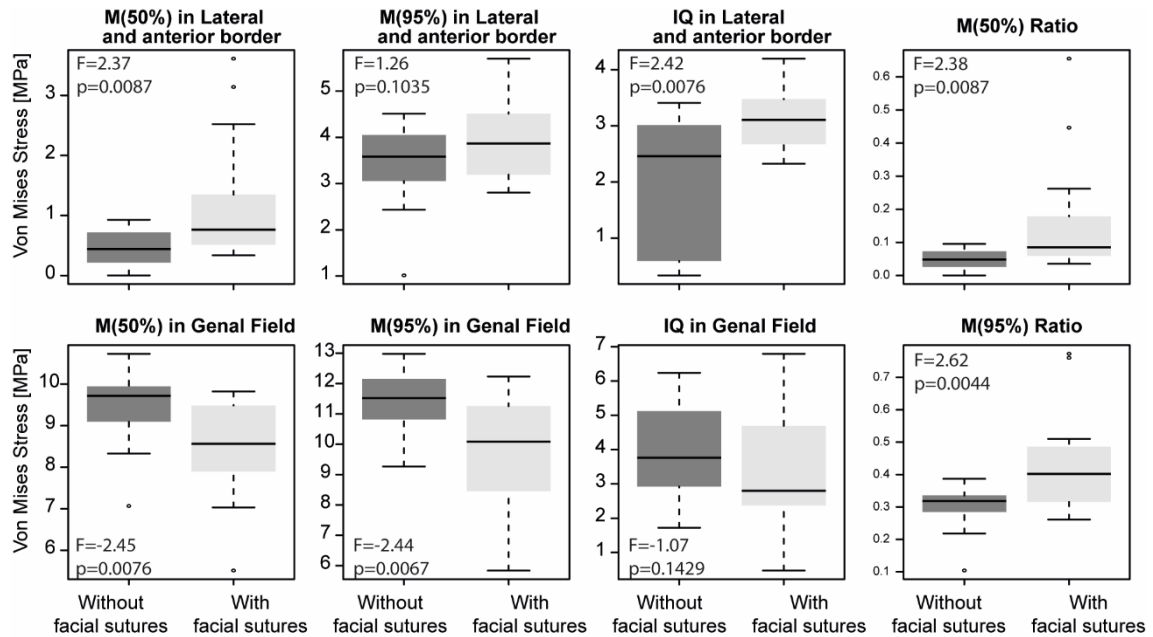
**Figure 5**. Box-plots of the median (M50), peak (M95) stress values and the Interquartile Range (IQR) for each FEA model in the  genal field (solved in analysis I) and in the anterior and lateral borders o (solved in analysis II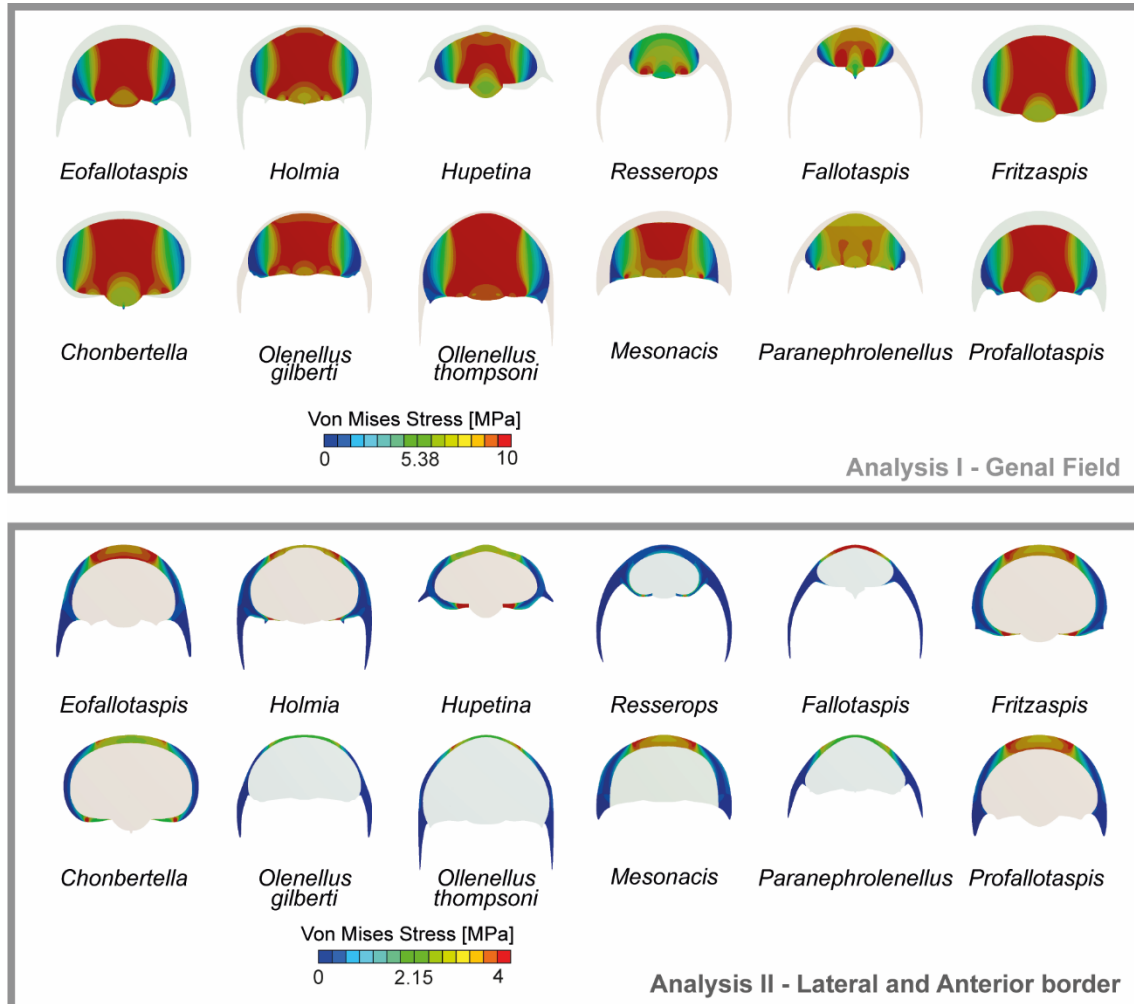) of all species grouped by the different suborders (Olenelliina, Redlichiina and Ptychopariina exclusively Cambrian and the suborden Asaphina). The Ratios are the comparison between the result obtained in the genal field (analysis I) and the anterior and lateral borders (analysis II) of M50 and M95 values. The median is the middle line of the box and whiskers represents the range. F and p-values of the Dunn's test with Bonferroni correction are included in each case.
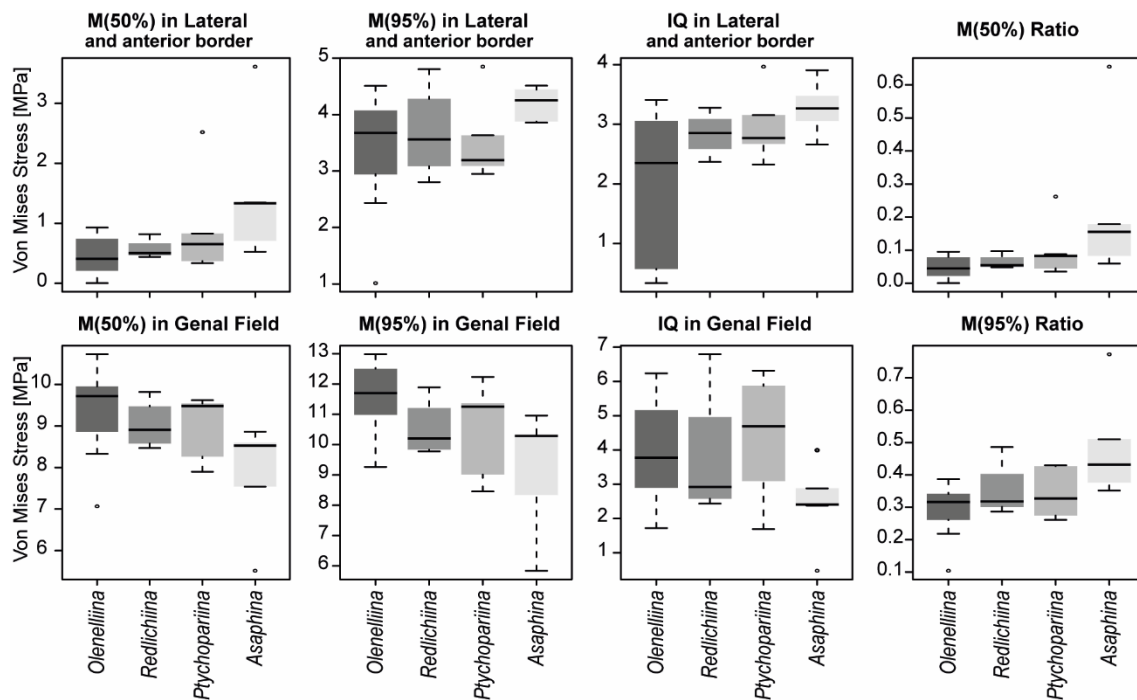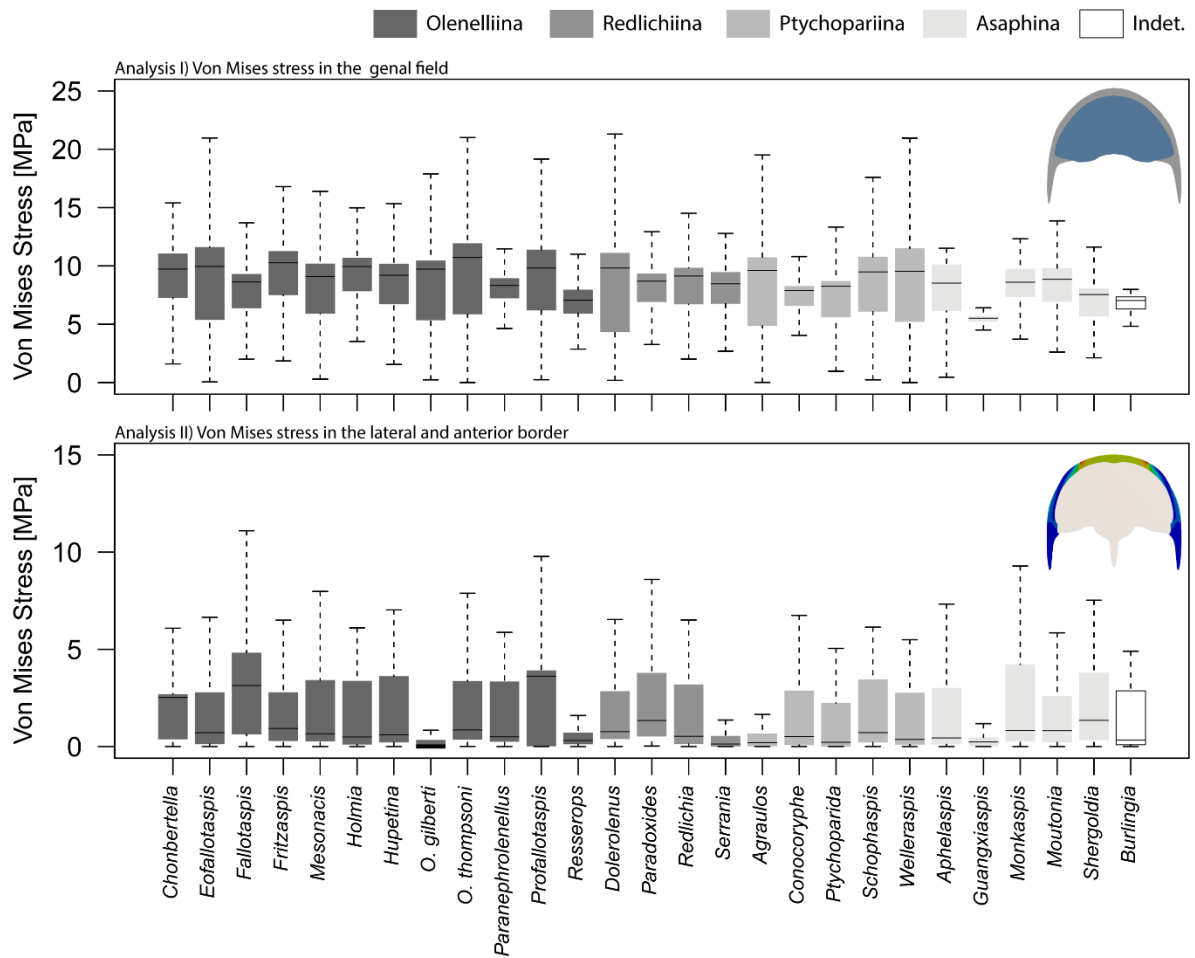
**SUPPLEMENTARY INFORMATION**

**Figure S1.** Box-plots of Von Mises stress values when QIM is assumed for each trilobite analysed when I) comparing genal field and II) comparing lateral and anterior border.

**Tables**

| TAXA | Series | Stage | Facial suture type | Suborder |
|------|--------|-------|--------------------|----------|
| *Agraulos* | Miaolingian | Drumian | Opisthoparian | Ptychopariina |
| *Aphelaspis* | Furongian | Paibian | Opisthoparian | Asaphina |
| *Burlingia* | Series 2 | Stage 4 | Proparian | Indet. |
| *Chonbertella* | Series 2 | Stage 3 | Lack | Olenelliina |
| *Conocoryphe* | Miaolingian | Drumian | Opisthoparian | Ptychopariina |
| *Dolerolenus* | Series 2 | Stage 4 | Opisthoparian | Redlichiina |
| *Eofallotaspis* | Series 2 | Stage 3 | Lack | Olenelliina |
| *Fallotaspis* | Series 2 | Stage 3 | Lack | Olenelliina |
| *Fritzaspis* | Series 2 | Stage 3 | Lack | Olenelliina |
| *Mesonacis* | Series 2 | Stage 3 | Lack | Olenelliina |
| *Guangxiaspis* | Furongian | Paibian | Opisthoparian | Asaphina |
| *Holmia* | Series 2 | Stage 4 | Lack | Olenelliina |
| *Hupetina* | Series 2 | Stage 3 | Lack | Olenelliina |
| *Monkaspis* | Miaolingian | Guzhangian | Opisthoparian | Asaphina |
| *Moutonia* | Miaolingian | Drumian | Opisthoparian | Asaphina |
| *Olenellus gilberti* | Series 2 | Stage 4 | Lack | Olenelliina |
| *O. thompsoni* | Series 2 | Stage 4 | Lack | Olenelliina |
| *Paradoxides* | Miaolingian | Drumian | Opisthoparian | Redlichiina |
| *Paranephrolenellus* | Series 2 | Stage 4 | Lack | Olenelliina |
| *Profallotaspis* | Series 2 | Stage 4 | Lack | Olenelliina |
| *Ptychopariina* | Miaolingian | Drumian | Opisthoparian | Ptychopariina |
| *Redlichia* | Series 2 | Stage 4 | Opisthoparian | Redlichiina |
| *Resserops* | Series 2 | Stage 3 | Lack | Olenelliina |
| *Schophaspis* | Miaolingian | Drumian | Opisthoparian | Ptychopariina |
| *Serrania* | Series 2 | Stage 3 | Opisthoparian | Redlichiina |
| *Shergoldia* | Furongian | Paibian | Opisthoparian | Asaphina |
| *Welleraspis* | Furongian | Paibian | Opisthoparian | Ptychopariina |

**Table S1**. List of the Cambrian trilobite genera used in this study.

| Taxa | Genal thinkness [mm] | Doublure thinkness [mm] | Width [mm] | Genal area [mm2] | Doublure area [mm2] | Burrowing force I [N] | Burrowing force II [N] |
|---|---|---|---|---|---|---|---|
| *Agraulos* | 0.17 | 0.3 | 25 | 214.12 | 52.66 | 24.96 | 11.42 |
| *Aphelaspis* | 0.02 | 0.04 | 25 | 198.47 | 65.13 | 2.83 | 1.69 |
| *Burlingia* | 0.01 | 0.015 | 25 | 99.341 | 161.37 | 1 | 1 |
| *Chonbertella* | 0.15 | 0.3 | 25 | 281.27 | 66.76 | 25.24 | 12.86 |
| *Conocoryphe* | 0.25 | 0.5 | 25 | 125.47 | 91.49 | 28.1 | 25.1 |
| *Dolerolenus sp.* | 0.15 | 0.4 | 25 | 225.11 | 99.93 | 22.58 | 20.99 |
| *Eofallotaspis* | 0.15 | 0.3 | 25 | 193.21 | 93.13 | 20.92 | 15.19 |
| *Fallotaspis* | 0.15 | 0.3 | 25 | 84.39 | 44.3 | 13.83 | 10.48 |
| *Fritzaspis* | 0.01 | 0.02 | 25 | 255.56 | 98.56 | 1.6 | 1.04 |
| *Mesonacis* | 0.01 | 0.02 | 25 | 177.72 | 80.57 | 1.34 | 0.94 |
| *Guangxiaspis* | 0.25 | 0.5 | 25 | 62.705 | 110.12 | 19.86 | 27.54 |
| *Holmia kjerulf* | 0.02 | 0.04 | 25 | 216.38 | 82.66 | 2.95 | 1.91 |
| *Hupetina* | 0.02 | 0.04 | 25 | 157.3 | 57.92 | 2.52 | 1.6 |
| *Monkaspis* | 0.01 | 0.02 | 25 | 201.02 | 117.46 | 1.42 | 1.14 |
| *Moutonia* | 0.01 | 0.02 | 25 | 194.78 | 86.89 | 1.4 | 0.98 |
| *Olenellus gilberti* | 0.01 | 0.02 | 25 | 198.2 | 36.97 | 1.41 | 0.64 |
| *O. thompsoni* | 0.01 | 0.02 | 25 | 296.21 | 43.32 | 1.73 | 0.69 |
| *Paradoxides* | 0.15 | 0.3 | 25 | 139.83 | 108.91 | 17.8 | 16.43 |
| *Paranephrolenellus* | 0.01 | 0.02 | 25 | 140.32 | 39.34 | 1.19 | 0.66 |
| *Profallotaspis* | 0.01 | 0.02 | 25 | 231.03 | 90.14 | 1.53 | 1 |
| *Ptychopariina* | 0.01 | 0.02 | 25 | 133.17 | 55.7 | 1.16 | 0.78 |
| *Redlichia* | 0.18 | 0.36 | 25 | 168.12 | 68.26 | 23.42 | 15.61 |
| *Resserops* | 0.01 | 0.02 | 25 | 84.418 | 82.2 | 0.92 | 0.95 |
| *Schophaspis* | 0.17 | 0.3 | 25 | 226.53 | 144.85 | 25.67 | 18.95 |
| *Serrania* | 0.01 | 0.02 | 25 | 175.47 | 53.27 | 1.33 | 0.77 |
| *Shergoldia* | 0.3 | 0.6 | 25 | 105.03 | 94.72 | 30.85 | 30.65 |
| *Welleraspis* | 0.2 | 0.4 | 25 | 250.55 | 67.68 | 31.76 | 17.27 |

**Table S2**. Geometric values of the FEA models - Average thickness of the genal field and the lateral and anterior border (in mm), area of the genal field and the lateral and anterior border (in mm2) and burrow force for the analysis I and II,

| Taxa | Nelements | MWAM | MWM | PeofAM | PEofM | M25 | M50 | M75 | M95 | Maximum axial stress |
|---|---|---|---|---|---|---|---|---|---|---|
| *Agraulos* | 34728 | 7.9327 | 9.4602 | 1.1617 | 1.6923 | 4.8549 | 9.6203 | 10.729 | 11.254 | 11.34 |
| *Aphelaspis* | 32201 | 7.9245 | 8.2489 | 0.5088 | 3.3906 | 6.1253 | 8.5286 | 10.1193 | 10.96 | 11.62 |
| *Burlingia* | 40484 | 6.8064 | 6.8434 | 0.0585 | 2.764 | 6.3135 | 7.0325 | 7.3521 | 7.501 | 7.52 |
| *Chonbertella* | 45194 | 8.7794 | 9.6407 | 0.5521 | 0.9073 | 7.2722 | 9.7282 | 11.056 | 11.878 | 12.10 |
| *Conocoryphe* | 51833 | 6.8505 | 7.6616 | 0.49 | 3.0855 | 6.58 | 7.898 | 8.2692 | 8.4544 | 8.30 |
| *Dolerolenus* | 95550 | 8.0507 | 9.4732 | 1.1847 | 3.6461 | 4.3201 | 9.8186 | 11.113 | 11.89 | 11.92 |
| *Eofallotaspis* | 79622 | 8.6604 | 9.7081 | 0.7084 | 2.6289 | 5.3772 | 9.9633 | 11.615 | 12.8688 | 12.38 |
| *Fallotaspis* | 35126 | 7.9146 | 8.2961 | 0.9354 | 3.9515 | 6.3813 | 8.6239 | 9.3046 | 12.9796 | 9.25 |
| *Fritzaspis* | 105158 | 9.1138 | 10.0287 | 0.4502 | 2.3658 | 7.5001 | 10.266 | 11.263 | 12.081 | 12.26 |
| *Mesonacis* | 72406 | 7.8232 | 9.0655 | 0.3718 | 0.321 | 5.9188 | 9.0946 | 10.19 | 10.819 | 10.97 |
| *Guangxiaspis* | 25388 | 5.3482 | 5.3474 | 0.1601 | 3.123 | 5.2188 | 5.5144 | 5.6933 | 5.8402 | 5.28 |
| *Holmia* | 89583 | 8.7847 | 9.7565 | 0.3924 | 1.941 | 7.8274 | 9.9459 | 10.698 | 11.404 | 11.53 |
| *Hupetina* | 65346 | 7.9593 | 8.9409 | 0.0721 | 2.8565 | 6.7306 | 9.1963 | 10.182 | 11.5172 | 10.37 |
| *Monkaspis* | 32386 | 8.1317 | 8.6594 | 0.2391 | 0.7407 | 7.3319 | 8.5953 | 9.7395 | 10.2972 | 10.42 |
| *Moutonia* | 31099 | 7.9801 | 8.8363 | 0.5629 | 0.3014 | 6.9337 | 8.8629 | 9.8131 | 10.289 | 10.38 |
| *Olenellus* | 80754 | 7.9508 | 9.3345 | 0.5996 | 4.0844 | 5.343 | 9.7158 | 10.465 | 11.153 | 11.27 |
| *O. thompsoni* | 122365 | 8.9533 | 10.4499 | 0.938 | 2.6518 | 5.8578 | 10.727 | 11.936 | 12.857 | 13.08 |
| *Paradoxides* | 58315 | 7.5396 | 8.3835 | 0.2186 | 3.6389 | 6.9098 | 8.6886 | 9.344 | 9.8868 | 10.00 |
| *Paranephrolenellus* | 22483 | 7.4915 | 8.1508 | 0.0524 | 2.1791 | 7.2173 | 8.3284 | 8.9379 | 9.2648 | 9.17 |
| *Profallotaspis* | 37339 | 8.5682 | 9.7502 | 0.6974 | 0.7402 | 6.1865 | 9.8224 | 11.388 | 12.152 | 12.19 |
| *Ptychopariina* | 342213 | 6.8326 | 7.8794 | 0.5494 | 4.8383 | 5.6049 | 8.2606 | 8.6958 | 9.0121 | 9.04 |
| *Redlichia* | 69091 | 7.9767 | 8.8114 | 0.5219 | 3.5831 | 6.7116 | 9.1271 | 9.8399 | 10.521 | 10.66 |
| *Resserops* | 35334 | 7.0289 | 7.113 | 0.4871 | 0.6633 | 5.9242 | 7.0659 | 7.9579 | 9.7613 | 7.95 |
| *Schophaspis* | 36399 | 8.2673 | 9.5072 | 0.7344 | 0.2599 | 6.0851 | 9.4825 | 10.776 | 11.36 | 11.46 |
| *Serrania* | 29173 | 7.6418 | 8.3163 | 0.6415 | 1.848 | 6.7554 | 8.47 | 9.472 | 9.7789 | 9.67 |
| *Shergoldia* | 43419 | 6.4887 | 7.2763 | 0.6786 | 3.6274 | 5.6868 | 7.5402 | 8.0624 | 8.3416 | 8.40 |
| *Welleraspis* | 40802 | 8.3462 | 9.408 | 1.2686 | 1.4441 | 5.2021 | 9.5439 | 11.517 | 12.232 | 12.27 |

**Table S3**. FEA results for the Analysis I: Number of mesh elements in the genal field (Nelements) and statistics: Mesh-Weighted Arithmetic Mean (MWAM), Mesh-Weighted Median (MWM), Percentage Error of the Arithmetic Mean (PEofAM), Percentage Error of the Median (PEofM) and the value quartiles (M25, M50, M75 and M95).

| Taxa | Nelements | MWAM | MWM | PeofAM | PEofM | M25 | M50 | M75 | M95 | Maximun axial stress |
|------|-----------|------|-----|--------|-------|-----|-----|-----|-----|----------------------|
| *Agraulos* | 239369 | 1.7995 | 2.4148 | 0.3525 | 4.4797 | 0.3707 | 2.523 | 2.6876 | 3.0917 | 2.74 |
| *Aphelaspis* | 10432 | 1.3528 | 0.7009 | 0.6291 | 1.1013 | 0.1258 | 0.7086 | 2.7865 | 3.8569 | 2.80 |
| *Burlingia* | 65409 | 2.9722 | 3.1644 | 0.884 | 0.7672 | 0.6282 | 3.1401 | 4.8243 | 5.703 | 5.01 |
| *Chonbertella* | 10660 | 1.482 | 0.9394 | 0.6484 | 1.1655 | 0.2859 | 0.9285 | 2.7854 | 3.3801 | 2.84 |
| *Conocoryphe* | 37053 | 1.5134 | 0.6487 | 0.3221 | 0.5214 | 0.268 | 0.6521 | 3.4212 | 3.6332 | 3.84 |
| *Dolerolenus* | 40255 | 1.3581 | 0.4916 | 0.8147 | 0.1711 | 0.0993 | 0.4925 | 3.3769 | 3.754 | 4.00 |
| *Eofallotaspis* | 37366 | 1.5834 | 0.5996 | 0.4066 | 1.1387 | 0.2126 | 0.6064 | 3.621 | 4.096 | 4.28 |
| *Fallotaspis* | 17951 | 0.8065 | 0.0026 | 0.4222 | 0.2229 | 0 | 0.0026 | 0.3363 | 4.5103 | 5.11 |
| *Fritzaspis* | 39640 | 1.6846 | 0.8708 | 0.3249 | 1.6099 | 0.3598 | 0.8568 | 3.3698 | 4.0513 | 3.63 |
| *Mesonacis* | 32492 | 1.3658 | 0.501 | 0.0451 | 0.2983 | 0.246 | 0.5025 | 3.348 | 3.7661 | 3.68 |
| *Guangxiaspis* | 278950 | 2.5142 | 3.3434 | 0.3541 | 8.0002 | 0.0114 | 3.6109 | 3.9181 | 4.5034 | 3.95 |
| *Holmia* | 33483 | 0.8641 | 0.3051 | 0.8384 | 3.2085 | 0.1185 | 0.3149 | 0.7112 | 3.5823 | 3.19 |
| *Hupetina* | 23543 | 1.5327 | 0.7469 | 0.7984 | 2.8198 | 0.3876 | 0.768 | 2.8479 | 4.455 | 3.18 |
| *Monkaspis* | 18634 | 2.0466 | 1.3745 | 0.9869 | 2.834 | 0.5235 | 1.3355 | 3.7894 | 4.4435 | 4.04 |
| *Moutonia* | 13769 | 1.3746 | 0.5227 | 0.1628 | 0.6792 | 0.1325 | 0.5262 | 3.1907 | 3.8779 | 3.34 |
| *Olenellus gilberti* | 93202 | 0.6033 | 0.1217 | 0.0576 | 4.6712 | 0 | 0.1274 | 0.5445 | 2.4291 | 2.27 |
| *O. thompsoni* | 17596 | 0.6874 | 0.2034 | 0.7818 | 0.3087 | 0.0104 | 0.2028 | 0.6687 | 3.0542 | 2.27 |
| *Paradoxides* | 43958 | 1.4546 | 0.5374 | 0.8411 | 4.445 | 0.0741 | 0.5135 | 2.8765 | 4.8036 | 4.23 |
| *Paranephrolenellus* | 6262 | 0.9156 | 0.2096 | 0.2981 | 2.5855 | 0.0031 | 0.215 | 2.2444 | 2.8309 | 2.33 |
| *Profallotaspis* | 14335 | 1.6678 | 0.7186 | 0.1398 | 0.0859 | 0.2154 | 0.718 | 3.4469 | 3.8819 | 3.91 |
| *Ptychopariina* | 62603 | 1.1496 | 0.3706 | 0.4721 | 0.1005 | 0.095 | 0.3703 | 2.7665 | 2.9487 | 2.98 |
| *Redlichia* | 27756 | 1.3134 | 0.4313 | 0.315 | 2.2923 | 0.1101 | 0.4412 | 3.0107 | 3.3675 | 3.19 |
| *Resserops* | 33068 | 0.3245 | 0.2225 | 1.3185 | 7.2969 | 0 | 0.2388 | 0.4693 | 1.0144 | 1.11 |
| *Schophaspis* | 22889 | 2.0588 | 0.8256 | 0.9079 | 0.5239 | 0.2674 | 0.8299 | 4.2324 | 4.8489 | 4.98 |
| *Serrania* | 8551 | 1.333 | 0.8005 | 0.0825 | 2.4249 | 0.2192 | 0.8199 | 2.5871 | 2.8045 | 2.58 |
| *Shergoldia* | 38138 | 2.0113 | 1.3625 | 0.207 | 1.16 | 0.3317 | 1.3467 | 3.8059 | 4.2555 | 4.37 |
| *Welleraspis* | 10717 | 1.0267 | 0.3497 | 0.7689 | 4.0338 | 0.0955 | 0.3356 | 2.8646 | 3.1937 | 3.08 |

**Table S3**. FEA results for the Analysis II: Number of mesh elements (Nelements) in the anterior and lateral borders and statistics: Mesh-Weighted Arithmetic Mean (MWAM), Mesh-Weighted Median (MWM), Percentage Error of the Arithmetic Mean (PEofAM), Percentage Error of the Median (PEofM) and the value quartiles (M25, M50, M75 and M95).